

the dynamics of oxygen precipitation. It was observed that, for short anneals at 700°C, the clusters are rapidly dissolved at higher temperatures because of insufficient size. An increase of the anneal time at 700°C and raising the temperature to 800°C multiplies the number of stable oxygen precipitates. However, it was found that the density for a given process temperature reaches a maximum that is independent of the nucleation conditions. This maximum decreases exponentially with increasing temperature, with an activation energy of 3.15 eV. The analysis of the bulk precipitate density after a CMOS cycle confirms that the maximum measured density of internal gettering sites in CZ silicon is determined by the highest process temperature to which the wafer is exposed.

Manuscript submitted Dec. 27, 1989; revised manuscript received May 30, 1990.

MEMC Electronic Materials assisted in meeting the publication costs of this article.

REFERENCES

1. S. M. Hu, *J. Appl. Phys.*, **52**, 3974 (1981).
2. J. G. Wilkes, *J. Cryst. Growth*, **65**, 214 (1983).
3. J. R. Patel, K. A. Jackson, and H. Reiss, *J. Appl. Phys.*, **48**, 5279 (1977).
4. C. Y. Kung, L. Forbes, and J. D. Peng, in "Defects in Silicon," (PV 83-9), W. M. Bullis, and L. C. Kimerling, Editors, p. 185, The Electrochemical Society

- Softbound Proceedings Series, Pennington, NJ (1986).
5. N. Inoue, K. Wada, and J. Osaka, in "Semiconductor Silicon 1981," (PV 81-5), H. R. Huff, R. J. Kriegler, and Y. Takeishi, Editors, p. 282, The Electrochemical Society Softbound Proceedings Series, Pennington, NJ (1981).
 6. K. Wada, H. Nakamishi, H. Takaoka, and N. Inoue, *J. Cryst. Growth*, **57**, 535 (1982).
 7. H. R. Huff, H. F. Schaake, T. T. Robinson, S. C. Baber, and D. Wong, *This Journal*, **130**, 1551 (1983).
 8. F. M. Livingston, S. Messoloras, R. C. Newman, B. C. Pike, R. J. Stewart, H. J. Binns, W. P. Brown, and J. G. Wilkes, *J. Phys. C*, **17**, 6253 (1984).
 9. M. Pagani and W. Huber, ESSDERC '87 (Bologna 1987), in "Solid State Devices," U. Soncini and P. Calzolari, Editors, p. 459, Elsevier Science Publications (1988).
 10. T. Y. Tan and C. Y. Kung, in "Semiconductor Silicon 1986," (PV 86-4), H. R. Huff, T. Abe, and B. Kolbesen, Editors, p. 864, The Electrochemical Society Softbound Proceedings Series, Pennington, NJ (1986).
 11. I. S. Lifshitz and V. Slyozov, *J. Phys. Chem. Solids*, **19**, 35 (1961).
 12. B. Craven, in "Semiconductor Silicon 1981," (PV 81-5), R. J. Kriegler and M. R. Hull, Editors, p. 254, The Electrochemical Society Softbound Proceedings Series, Pennington, NJ (1981).

Characterization of Silane-Reduced Tungsten Films Grown by CVD as a Function of Si Content

M. Suzuki,¹ N. Kobayashi, and K. Mukai

Central Research Laboratory, Hitachi, Limited, Higashi-koigakubo, Kokubunji, Tokyo 185, Japan

S. Kondo

Advanced Research Laboratory, Hitachi, Limited, Higashi-koigakubo, Kokubunji, Tokyo 185, Japan

ABSTRACT

Tungsten (W) films grown by low-pressure chemical vapor deposition using tungsten hexafluoride (WF_6) and silane (SiH_4) are characterized as a function of the Si content ($[Si]$) in the films. The electrical resistance, stress, and composition of as-deposited films showed a strong dependence on $[Si]$ and could be classified into three groups: $[Si] \leq 2$ atom percent (a/o), $2 \leq [Si] < 20$ -40 a/o, and $[Si] > 40$ a/o. When $[Si] \leq 2$ a/o, the electrical resistance is approximately proportional to $[Si]$, and is mainly determined by impurity scattering of Si. In this $[Si]$ region, W can be selectively deposited on Si. When $2 \leq [Si] < 20$ -40 a/o, the temperature dependence of electrical resistance is characteristic of semiconductors, and a substantial increase in superconducting transition temperature ($T_c = 4.4$ K) is observed. When $[Si] > 40$ a/o, microcrystals of WSi_2 begin to form. These results are discussed in terms of a model based on the solubility of Si in W.

Tungsten (W) and tungsten silicide (WSi_2) have been used for gate and interconnect metals in silicon (Si) ultra-large scale integration (ULSI) because of their low resistivity and high resistance to stress-migration and electromigration (1-3). Low-pressure chemical vapor deposition (LPCVD), using tungsten hexafluoride (WF_6) and silane (SiH_4), has been used for deposition of these films (4-6). Recently, it was discovered that W can be selectively deposited on Si or metal using LPCVD with an appropriate gas flow ratio of WF_6/SiH_4 (7, 8). Since then, selective W deposition has been extensively investigated for submicron contact and/or via filling. In spite of the growing demand for this technology in practical applications, little work has been performed (9) on the characterization of films deposited with WF_6/SiH_4 , and there is still no comprehensive understanding of the properties of these films. For example, issues such as reduction of film resistivity and film stress, and control of selective or non-selective W deposition, have become serious problems in LPCVD of W and WSi_2 .

The purpose of this study is to clarify the physical factors that determine these film properties. In this work, a set of tungsten films grown by LPCVD under various processing parameters is characterized in terms of electrical resistance, film stress, film composition, etc. As a result, Si content, hereafter denoted by $[Si]$, has been found to correlate strongly with film morphology, electrical resistance, and stress. A drastic change in these characteristics is observed at $[Si] \approx 2$ a/o. Moreover, deposition of W gradually changes from selective to non-selective as $[Si]$ increases. The structure of Si in W is examined using scanning electron microscopy (SEM), transmission electron microscopy (TEM), x-ray diffraction (XRD), and Auger electron spectroscopy (AES). The results are related to film porosity and low-temperature electrical resistance.

Experimental

Phosphorus-doped, (100)-oriented, 4-in. Si wafers with a resistivity of 10-15 Ω -cm were used for blanket LPCVD deposition of W. Prior to W deposition, native oxide on the Si substrates was removed by etching in a hydrofluoric acid (HF) solution. The blanket films thus produced were

¹ Present address: Semiconductor Design and Development Center, Hitachi, Limited 20-1, Josuihoncho 5 Chome, Kodaira-shi, Tokyo 187, Japan.

Table I. Summary of the CVD conditions and film characteristics of the W CVD films

Sample no.	CVD conditions					Temperature (°C)	Si content (AES) a/o	Resistivity ($\mu\Omega\text{cm}$)	Detected phases (XRD)
	WF ₆	SiH ₄	Ar	N ₂ mtorr	H ₂				
1	40	40	170	400	0	228	3.5	118	α -W
2	40	20	190	400	0	236	1.5	60.2	α -W
3	40	30	180	400	0	236	1.6	64.7	α -W
4	40	60	150	400	0	236	3.5	217	α -W
5	40	80	130	400	0	236	16.1	214	α -W + β -W
6	40	120	90	400	0	236	43.8	163	α -W + β -W + (WSi ₂)
7	40	40	170	400	0	266	1.4	73.6	α -W
8	40	40	170	400	0	281	1.1	75.5	α -W
9	40	40	170	400	0	295	0.65	40.8	α -W
10	40	40	170	400	0	324	0.45	26.0	α -W
11	40	15	195	400	0	354	0.20	10.0	α -W
12	40	20	190	400	0	354	0.27	13.8	α -W
13	40	30	180	400	0	354	0.29	16.1	α -W
14	40	40	170	400	0	354	0.40	16.8	α -W
15	40	60	150	400	0	354	4.0	365	α -W + β -W
16	40	80	130	400	0	354	13.6	205	α -W + β -W
17	40	120	90	400	0	354	43.1	257	α -W + β -W + (WSi ₂)
18	40	40	70	0	200	286	1.1	61.2	α -W
19	40	20	90	0	200	350	0.22	18.0	α -W
20	40	40	70	0	200	350	0.58	28.2	α -W
21	40	80	30	0	200	350	6.2	325	α -W + β -W
22	40	40	70	0	200	404	0.38	16.4	α -W

used to perform electrical resistivity measurements and characterization studies. On the other hand, wafers with patterned oxides were prepared to evaluate the selectivity of W deposition. Submicron contacts were defined on CVD oxide deposited on Si wafers. W CVD was performed in a cold-wall-type LPCVD reactor, using WF₆, SiH₄, N₂, Ar, and H₂ at temperatures in the range 228°-404°C. In this apparatus, the temperature of the wafer susceptor was monitored by an infrared pyrometer. The inlet gas flows of WF₆ and SiH₄ were 80 and 30-240 cm³/min, respectively. These gases were diluted with Ar, and N₂ or H₂, so that the total pressure and total gas flow were fixed. The deposition time ranged from 6 to 12 min. The CVD conditions and film characteristics are summarized in Table I.

Electrical resistance was measured with the four-point probe method in the temperature region 2.1-300 K. The samples were cut into approximately 3-mm × 10-mm chips, and copper lead wires were attached to the W film surfaces using indium ingots. Electrical resistivity was calculated from film thickness and sheet resistance. The W film thickness was measured by cross-sectional SEM. The film stress σ was calculated from the vertical displacement

of the substrate δ at a distance L from the center of the substrate and the W film thickness, d , using the following equation

$$\sigma = Et^2\delta / \{6(1-\nu)L^2d\} \quad [1]$$

where E is Young's modulus, ν is Poisson's ratio, and t is the substrate thickness, all for the Si substrate. The curvature of the wafer was measured by a laser-scanning curvature measurement apparatus.

The W films were analyzed by TEM, AES, and XRD. The cross-sectional TEM observation of W films was executed with an accelerating voltage of 200 keV (Hitachi H-800). The crystal phase was identified by XRD analysis (Regaku-denki RAD Type-3 diffractometer) using the CuK α line. The Si content was measured by AES after Ar sputtering of the W surfaces, because the W surface was contaminated with oxygen and carbon, and Si generally segregates at the surface. The AES analysis was performed using a cylindrical mirror Auger spectrometer (PHI, Model 10-155, Perkin-Elmer) with an accelerating voltage of 5 keV. The W films were sputtered using Ar ions with a primary energy of 3.5 keV. The typical sputtering rate of W was 3 nm/min. The Si content and other impurity concentrations were obtained using AES sensitivity coefficients. The sensitivity coefficient of Si_{L,VV} was recalibrated using standard samples of WSi_x ($x = 2.3$ and 2.5), where the x

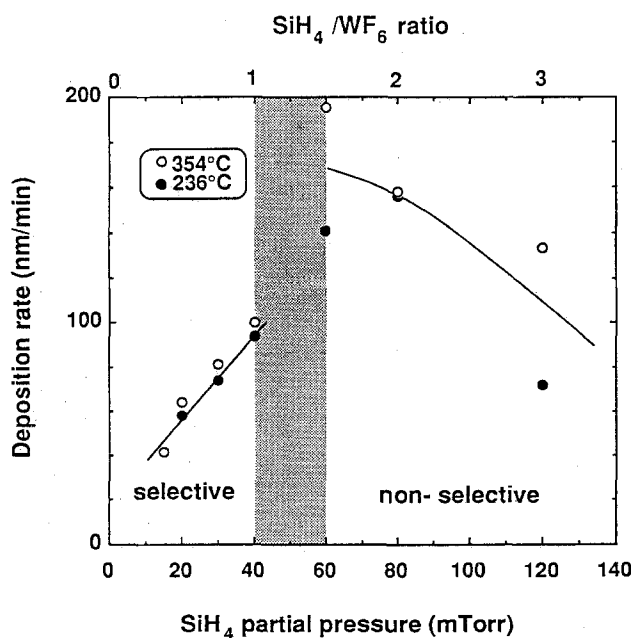


Fig. 1. Dependence of deposition rate of W film on partial pressure of SiH₄. Inlet gases were diluted with Ar and N₂. Open and solid circles represent data of W deposition at 354°C and 236°C, respectively.

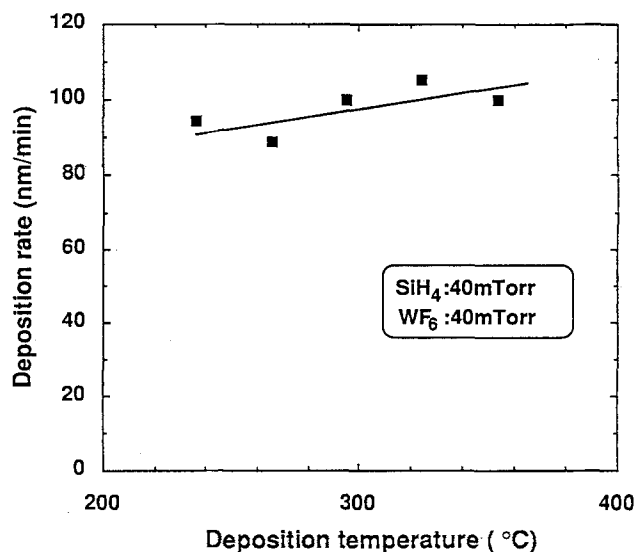


Fig. 2. Dependence of deposition rate of W film on temperature (in selective deposition of W). Inlet gases were diluted with Ar and N₂.

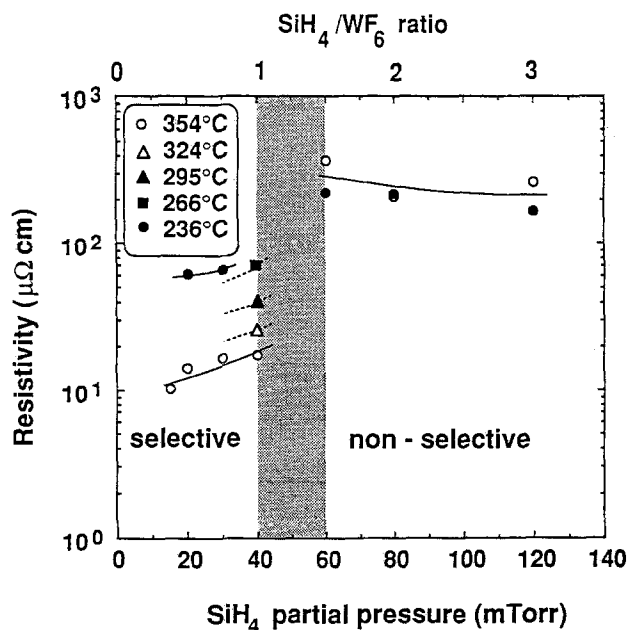


Fig. 3. Dependence of electrical resistivity of W film on partial pressure of SiH_4 . The horizontal axis above represents the inlet gas flow ratio of SiH_4/WF_6 . Inlet gases were diluted with Ar and N_2 .

values were determined from Rutherford backscattering (RBS) measurement. The x values obtained by AES were about 5% lower than the RBS results. For small Si content (<5%), some AES results were compared with corresponding secondary ion mass spectroscopy (SIMS) profiles of the samples. As a result, a linear relationship between the two data was obtained within an experimental error of 20%. Carbon and nitrogen were detected only at W surfaces. A small amount of oxygen and fluorine (<0.5 a/o), in addition to Si, were detected in the films. The AES peak of fluorine was observed to decrease during primary electron beam irradiation on the W surface. Thus, we do not believe that a fluorine concentration of less than 0.5 a/o is rigidly correct.

The grain sizes of W polycrystals, D , were estimated from the peak width of α -W (110) XRD spectra using Sherrer's formula (10)

$$D = 0.94\lambda / (B - b) \cos \theta \quad [2]$$

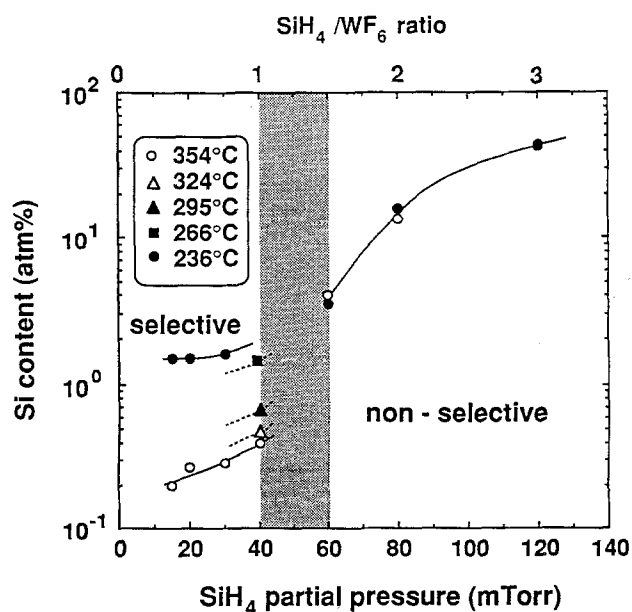


Fig. 4. Dependence of Si content in W film on partial pressure of SiH_4 . The horizontal axis above represents the inlet gas flow ratio of SiH_4/WF_6 . Inlet gases were diluted with Ar and N_2 .

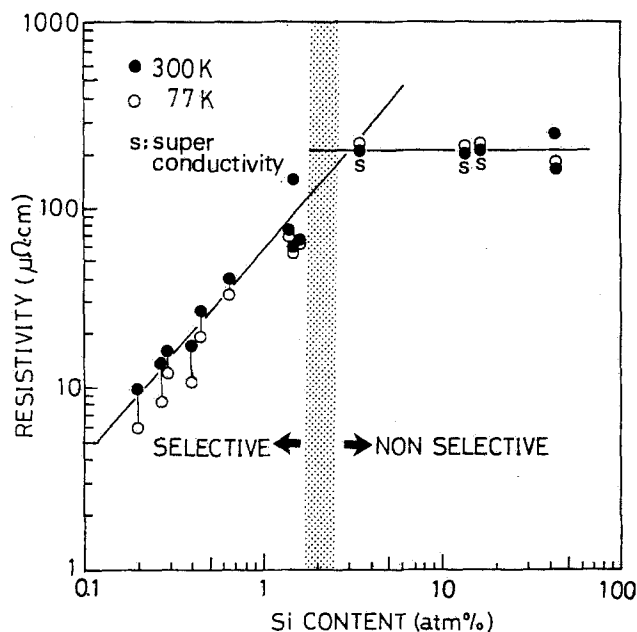


Fig. 5. Relation between electrical resistivity of W film and Si content. Solid and open circles represent the electrical resistivity at 300 K and 77 K, respectively.

where λ , θ , B , and b are the x-ray wavelength, the Bragg angle, the line breadth, and the instrumental broadening, respectively. The value of b was estimated from the breadth of the diffraction peaks for the Si single crystal. The mass density was measured from the film thickness and weight of W films.

Results

Deposition rate.—The dependence of deposition rate on the partial pressure of SiH_4 (P_{SiH_4}) is shown in Fig. 1. The deposition rate is proportional to P_{SiH_4} when the flow ratio of WF_6/SiH_4 is less than 1. W can be deposited selectively on Si in this WF_6/SiH_4 region. When WF_6/SiH_4 exceeds 1, the deposition rate is a maximum at around $\text{WF}_6/\text{SiH}_4 = 1.5$, and decreases with increasing P_{SiH_4} . The dependence of deposition rate on temperature is shown in Fig. 2. At $\text{WF}_6/\text{SiH}_4 = 1$, where selective W deposition occurs, the deposition rate is only slightly affected by temperature. These results show that the W growth is limited by mass transfer of SiH_4 .

Electrical resistivity and Si content.—The dependence of electrical resistivity (ρ) on P_{SiH_4} is shown in Fig. 3. The growth temperatures ranges from 236° to 354°C. One notes that ρ is strongly affected by temperature when WF_6/SiH_4

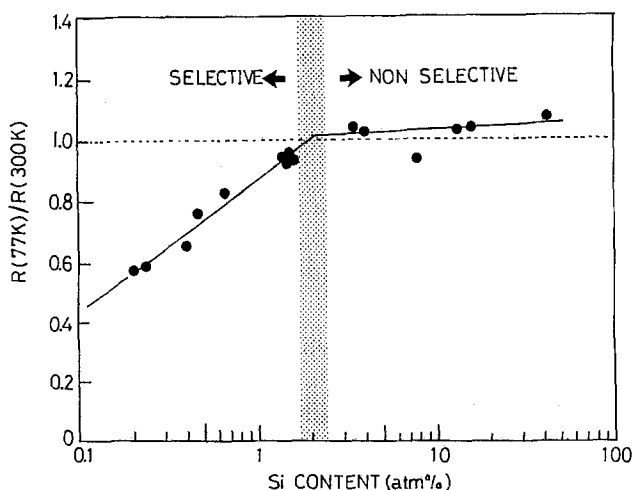


Fig. 6. Relation between the resistivity ratio, $\rho(77\text{ K})/\rho(300\text{ K})$, and Si content.

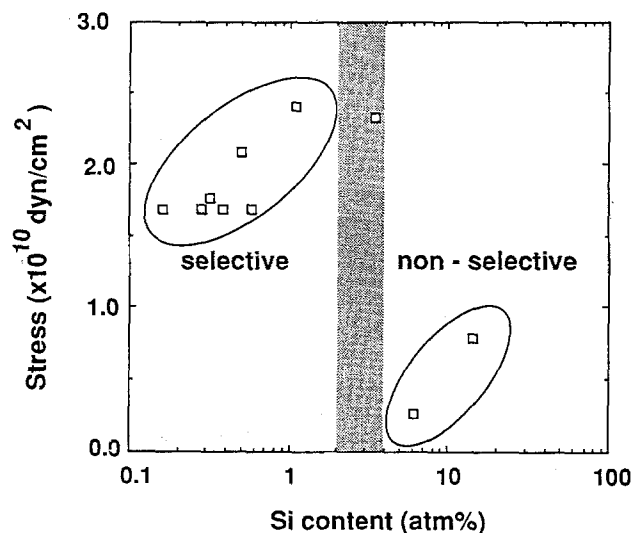
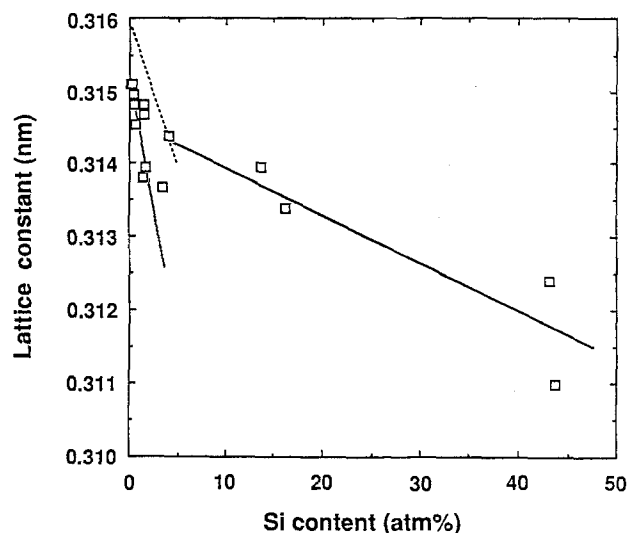


Fig. 7. Relation between stress of W film and Si content

Fig. 9. Dependence of lattice constant of α -W on Si content

is less than 1. However, it is only slightly affected when $W\phi/SiH_4$ is higher than 1, although ρ increases slightly with P_{SiH_4} . The Si content in the films varied with the deposition conditions, as shown in Table I. The Si contents of the same samples are plotted in Fig. 4. It should be noted that dependence of [Si] on P_{SiH_4} coincides fairly well with that of ρ , as shown in Fig. 3 and 4. This result indicates that electrical resistivity ρ is well characterized with respect to [Si]. In fact, there is a strong dependence of ρ on [Si], as shown in Fig. 5. When [Si] \leq 2 a/o, ρ is almost proportional

to [Si] and W could be selectively deposited on Si. On the other hand, when [Si] \geq 2 a/o, most of the selectivity is lost, and ρ is only slightly affected by [Si].

The temperature dependence of ρ also differs appreciably in the [Si] \leq 2 a/o region vs. the [Si] \geq 2 a/o region. In all the samples, the electrical resistivity at 77 K, $\rho(77\text{ K})$, equaled a residual resistivity, because ρ saturated around 77 K. The resistivity ratio of $\rho(77\text{ K})/\rho(300\text{ K})$ is plotted as a function of [Si] in Fig. 6. When [Si] \leq 2 a/o, the ratio is less than 1 (i.e., ρ decreases with decreasing temperature), and the residual resistivity was proportional to [Si]. When [Si] \geq 2 a/o, the ratio is higher than 1 (i.e., ρ increases with decreasing temperature). This temperature dependence is characteristic of semiconductors rather than metals. The W films with [Si] = 3.5, 13.6, and 16.1 a/o showed superconducting behavior at 4.4 K (11). The superconducting transition temperature (T_c) of 4.4 K is much higher than that of the bulk W (0.012 K) reported in the literature (12). Also, the superconducting transition was not observed until 2 K for samples with [Si] \leq 2 a/o or [Si] $>$ 40 a/o.

Film stress.—The film stress σ also depends on [Si], as shown in Fig. 7. For [Si] \leq 2 a/o, σ is tensile stress and it increases with [Si], whereas, when [Si] \geq 2 a/o, σ becomes low. The maximum stress was at around [Si] \approx 2 a/o.

Phase identification in the films.—The XRD spectra of the W films are shown as a function of [Si] in Fig. 8. The

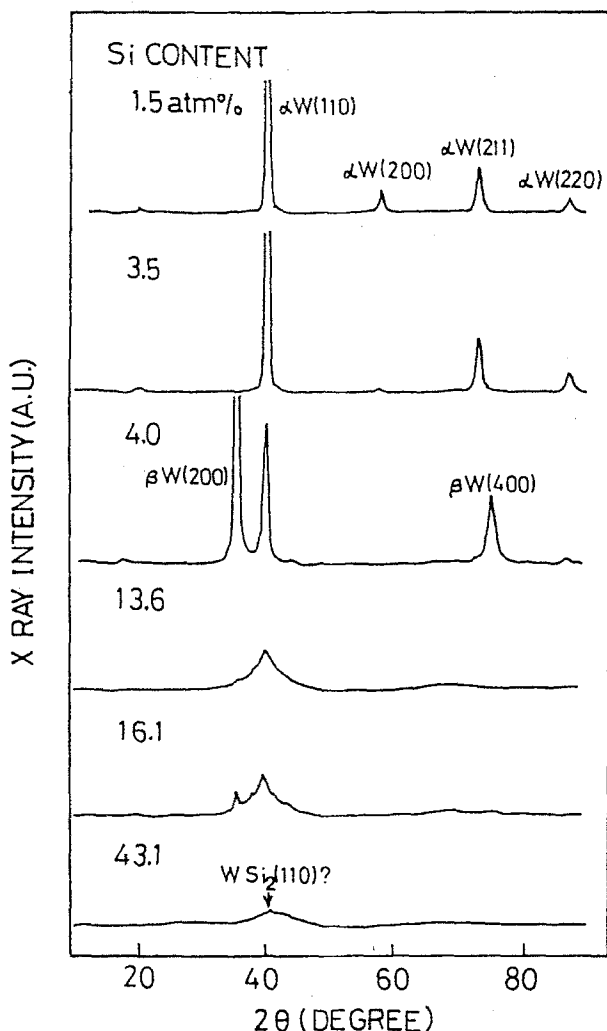
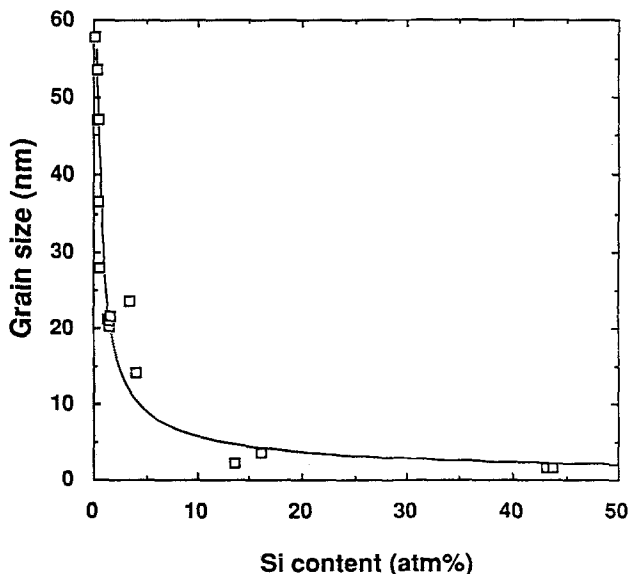


Fig. 8. XRD spectra of W films with various Si contents

Fig. 10. Dependence of grain size of α -W on Si content

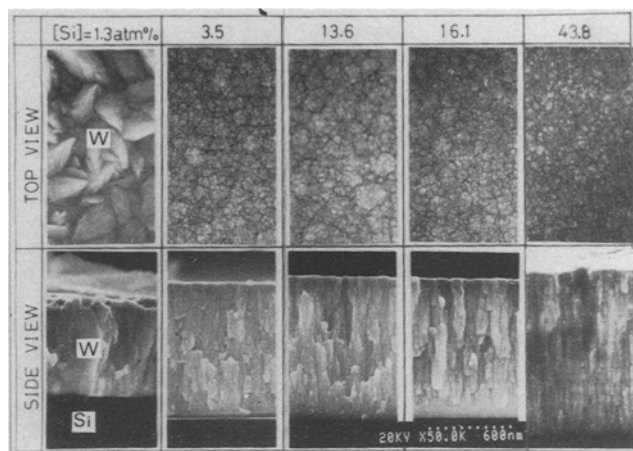


Fig. 11. SEM micrographs of W films with various Si contents

XRD analysis shows that the films with $[Si] \leq 2$ a/o consist of α -W polycrystals. When $[Si] \geq 2$ a/o, α -W peaks become broad and new β -W peaks appear. The β -W phase is known to be a metastable phase of W. When $[Si] > 40$ a/o, broad WSi_2 peaks appear together with α -W and β -W peaks. To analyze the crystal structure of W in more detail, the lattice constant and grain size of α -W were measured from the Bragg angle and the peak width of α -W (110), respectively. The lattice constants and the grain sizes are plotted against $[Si]$ in Fig. 9 and Fig. 10, respectively. The lattice constant of α -W decreased from 0.316 nm to 0.314 nm, and grain sizes rapidly decreased with increasing $[Si]$ from 0.27 to 1.6 a/o. In Fig. 9, the broken line represents the lattice constants of the W films free from stress. These values were calculated from the experimental data by subtracting the effect of tensile stress on the lattice constant. The lattice constant as well as grain size decreased slightly, with $[Si] \geq 2$ a/o. In this region, the lattice constants of β -W decreased from 0.500 to 0.495 nm with increasing $[Si]$ from 4.0 to 16.1 a/o.

Film morphology.—SEM micrographs of the films are shown in Fig. 11. The film morphology drastically changed around $[Si] \approx 2$ a/o. The W films with $[Si] \leq 2$ a/o had an equi-axed structure with large grains. On the other hand, when $[Si] \geq 2$ a/o, the W films had a fine columnar structure with small grains.

The W films with $[Si] \leq 2$ a/o had a slightly lower mass density (17-18 g/cm³) than bulk W (19.2 g/cm³). When $[Si] \geq 2$ a/o, the mass density was 13-15 g/cm³, and the porosity of these films was recognized in SEM. The cross sectional TEM micrographs with electron diffraction patterns of the sample with $[Si] = 1.3$ and 13.6 a/o are shown in Fig. 12. As shown in the TEM micrographs, the large W grains were observed in the sample with $[Si] = 1.3$ a/o. On the other hand, micro-channels were observed between the fine columnars in the sample with $[Si] = 13.6$ a/o. The existence of micro-channels in the films can explain the porosity of the films with $[Si] \geq 2$ a/o.

Discussion

The electrical resistance and other film properties can be categorized by $[Si]$ into three groups: $[Si] \leq 2$ a/o, $2 \leq [Si] < 20$ -40 a/o, and $[Si] > 40$ a/o. The characteristics of each group are summarized in Table II. When $[Si] \leq 2$ a/o, ρ

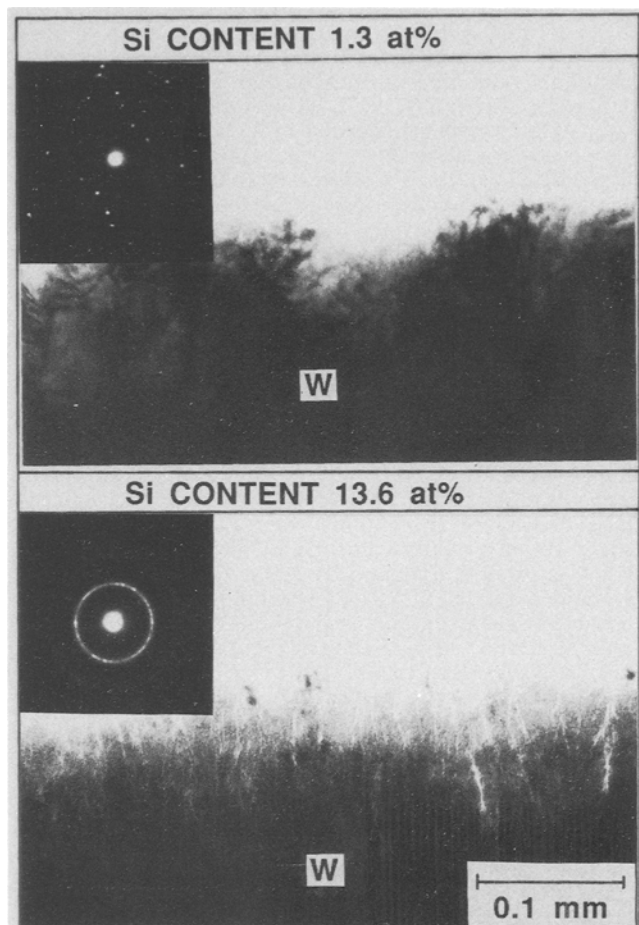
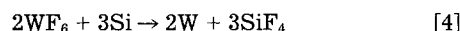


Fig. 12. Cross-sectional TEM micrographs with electron diffraction patterns of W films with Si content of 1.3 and 13.6.

decreased with $[Si]$ and the residual resistivity was proportional to $[Si]$. The XRD analysis showed that the films consist of α -W polycrystals, and that a lattice constant of W decreased with increasing $[Si]$. These results indicate that for $[Si] \leq 2$ a/o, Si dissolves substitutionally in W, and that ρ is mainly determined by the impurity scattering of Si. In the selective deposition of W, one possible chemical reaction is



In this $[Si]$ region, the deposition rate of W was proportional to P_{SiH_4} . This result indicates that the growth kinetics are limited through the reduction of WF_6 by Si-containing species. The most probable representation of this result is chemical reaction [4]. The catalytic action of the W surface for the decomposition of SiH_4 has been discussed by several authors (9, 13, 14). They reported that a monolayer of Si was formed on the W surface after the W film was exposed to SiH_4 at around 300°C. A clear explanation of the decomposition mechanism has not been obtained. However, our experimental results strongly indicate that the decomposition of SiH_4 (3) occurs preferentially at W

Table II. Summary of film characteristics with respect to Si content in the W CVD films

Si content	Selectivity	Electrical resistance	Superconductivity	Stress	Identified phases	Film morphology
$[Si] \leq 2$ a/o	Yes	$\rho \propto [Si]$ "metallic"	$T_c < 2$ K	$\sigma > 10^{10}$ dyn/cm ² increase with $[Si]$	α -W	equi-axed with large grain
$2 \leq [Si] < 20$ -40			$T_c = 4.4$ K		α -W α -W + β -W	columnar with small grain
$[Si] > 40$	No	$\rho \approx \text{const}$ "semiconductor"	$T_c < 2$ K	$\sigma < 10^{10}$ dyn/cm ²	α -W + β -W + WSi_2	

surfaces, rather than at oxide surfaces. This follows from our experimental results showing that selective W deposition leads to Si incorporation in the W film, and Si is substitutionally dissolved in W in the film. Therefore, in the selective deposition of W, SiH₄ is decomposed at W surfaces to the extent that it can dissolve in W. Otherwise, when decomposed Si at W surfaces exceeds the solubility in W, undissolved Si can form a reactive species such as radicals, which make W nuclei even on the oxide (*i.e.*, selectivity loss).

On the other hand, when $2 \leq [\text{Si}] < 20\text{-}40$ a/o, most of the selectivity was lost, and ρ was only slightly affected by [Si]. It should be noted that a superconducting transition temperature, T_c , increased markedly. The temperature dependence of ρ is characteristic of semiconductors rather than metals. In this [Si] region, the films consist of α -W and β -W microcrystals, and film morphology is characterized by a fine columnar structure with small grains. The grain sizes, estimated by the XRD peak width of α -W (110) using Sherrer's relation, were 12, 2, and 3 nm in the W films with concentrations of 3.5, 13.6, and 16.1 a/o, respectively. The mass density of these films was 13-15 g/cm³, which is smaller than the bulk value. Silicides of W₅Si₃ and WSi₂, which are thermodynamically stable in this region, were not detected in the films, which strongly indicates that undissolved Si segregates at grain boundaries. This interpretation is supported by the experimental results of Si solubility in W (5.5 a/o at 1800°C) (15).

The stresses of the W films were tensile, and they decreased when [Si] ≥ 2 a/o. This stress relaxation is probably related to a small-grain and to fine columnar W film structures with Si segregation at W grain boundaries. When [Si] > 40 a/o, XRD analysis of the films showed broad peaks of WSi₂ along with α -W and β -W. The peaks of WSi₂ were very broad in as-deposited films, as shown in Fig. 8. However, the existence of WSi₂ was clarified by the sharp XRD peaks of WSi₂ in the films when annealed in H₂ at 500°C for 1h. These results indicate that as-deposited films contain microcrystals of WSi₂. This is the important difference between these films and the films with $2 \leq [\text{Si}] < 20\text{-}40$ a/o.

Conclusion

W films grown by LPCVD using WF₆ and SiH₄ were characterized as a function of Si content in the films. Film electrical resistance, stress, and morphology are strongly dependent on [Si]. The films can be categorized as a function of [Si] into three groups: [Si] ≤ 2 a/o, $2 \leq [\text{Si}] < 20\text{-}40$ a/o, and [Si] > 40 a/o. When [Si] ≤ 2 a/o, Si dissolves substitutionally in α -W, and the electrical resistivity is determined by the impurity scattering of Si. In this region, selective deposition of W can be achieved. When $2 \leq [\text{Si}] < 20\text{-}40$ a/o, the films consist of β -W in addition to α -W, and undissolved Si can segregate at the grain boundary of the W polycrystal. The selectivity loss of W CVD is probably related to the solubility limit of Si in W. The film morphology is characterized by a fine columnar structure with small grains. The tensile stress of the films was large

(>10¹⁰ dyne/cm²), and decreased with increasing [Si]. A high T_c of 4.4 K was observed, and the temperature dependence of electrical resistance is characteristic of semiconductors. Finally, when [Si] > 40 a/o, microcrystals of WSi₂ began to form in the films. A high T_c was not observed in these samples.

Acknowledgments

The authors would like to acknowledge Dr. M. Matsui for providing the experimental apparatus for low-temperature electrical resistance measurements, Dr. M. Naito for T_c measurements, and T. Ishiba for XRD analysis of W films. They are also much indebted to Drs. H. Sunami, S. Iwata, N. Yamamoto, K. Hinode, and Y. Homma, with Central Research Laboratory, and T. Kobayashi with Advanced Research Lab, and to N. Ohwada with Device Development Center, and Y. Sakai with Musashi Works, Hitachi, Ltd., for their discussions and encouragement during the course of this work.

REFERENCES

1. D. M. Brown, W. E. Engeler, M. Garfinkel, and P. V. Gray, *Solid State Electron.*, **11**, 1105 (1968).
2. S. Iwata, N. Yamamoto, N. Kobayashi, and T. Terada, *IEEE Trans. Electron Devices*, **ED-31**, 1174 (1984).
3. M. Y. Tsai *et al.* *This Journal*, **128**, 2207 (1981).
4. J. S. Lo, R. W. Haskell, J. G. Bryne, and A. Sosin, "Chemical Vapor Deposition," Fourth International Conference, G. F. Wakefield and J. M. Blocher, Jr., Editors, p. 74, The Electrochemical Society, Pennington, NJ (1973).
5. D. L. Brors, J. A. Fairs, K. A. Monnig, and K. C. Saraswat, in "Chemical Vapor Deposition," (PV 84-6), M. Robinson, C. H. J. Brekel, G. W. Cullen, J. M. Blocher, Jr., and P. Rai-Choudhury, Editors, p. 275, The Electrochemical Society Softbound Proceedings Series, Pennington, NJ (1984).
6. N. Kobayashi, N. Hara, S. Iwata, and N. Yamamoto, Proc. of IEEE VLSI Multilevel Interconnect. Conf., p. 436 (1986).
7. T. Ohba, S. Inoue, and M. Maeda, Proc. IEEE Electron Devices Meeting, p. 213 (1987).
8. H. Kotani, T. Tsutsumi, J. Komori, and S. Nagano, *ibid.*, p. 217.
9. J. E. J. Schmitz, M. J. Buting, and R. C. Ellwanger, Proc. of the Workshop on Tungsten and Other Refractory Metals for VLSI Application IV, R. S. Blewer and C. M. McConica, Editors, p. 27, Material Research Society, Pittsburgh, PA (1989).
10. H. Oikawa and T. Tsuchiya, *J. Vac. Sci. Technol.*, **5**, 1153 (1977).
11. N. Kobayashi, M. Suzuki, and S. Kondo, Submitted to *Appl. Phys. Lett.*
12. J. W. Gibson and R. A. Hein, *Phys. Rev. Lett.*, **12**, 688 (1964).
13. M. L. Yu and B. N. Eldridge, *J. Vac. Sci. Technol.*, **A7**, 625 (1989).
14. L. H. Dubois and R. G. Nuzzo, *J. Vac. Sci. Technol.*, **A2**, 441 (1984).
15. M. Hansen, "Constitution of Binary Alloys," p. 1203, McGraw-Hill Co., New York (1958).